Flash-evaporation of oxidizer spray during start-up of a spacecraft engine in vacuum

R. Schmehl, J. Steelant

roland.schmehl@esa.int
Aerothermodynamics Section TOS-MPA/ESTEC, European Space Agency,
Noordwijk, The Netherlands

The low-pressure oxidizer preflow during start-up of a hypergolic spacecraft engine is analyzed computationally. An iterative Euler-Lagrange approach is used to describe the three-dimensional two-phase flow of oxidizer vapour and spray characterized by intense phase transfer. Multipoint injection and flash-atomization of liquid oxidizer is modelled by stochastic droplet injection according to injector locations and spray characteristics. Based on the framework of classical D^2-theory, a flash-evaporation model is developed to describe heat and mass transfer of superheated liquid droplets. The computed transsonic flow field agrees well with experimental characteristics such as pressure level and temperature decrease and further provides detailed local information on vapour flow homogeneity and liquid wall deposit.

1 Introduction

During start-up of a hypergolic spacecraft engine under vacuum conditions, a steady flow of vaporizing liquid oxidizer is maintained in the combustion chamber to ensure well-defined conditions prior to injection of liquid fuel and hypergolic ignition. Due to the absence of com-

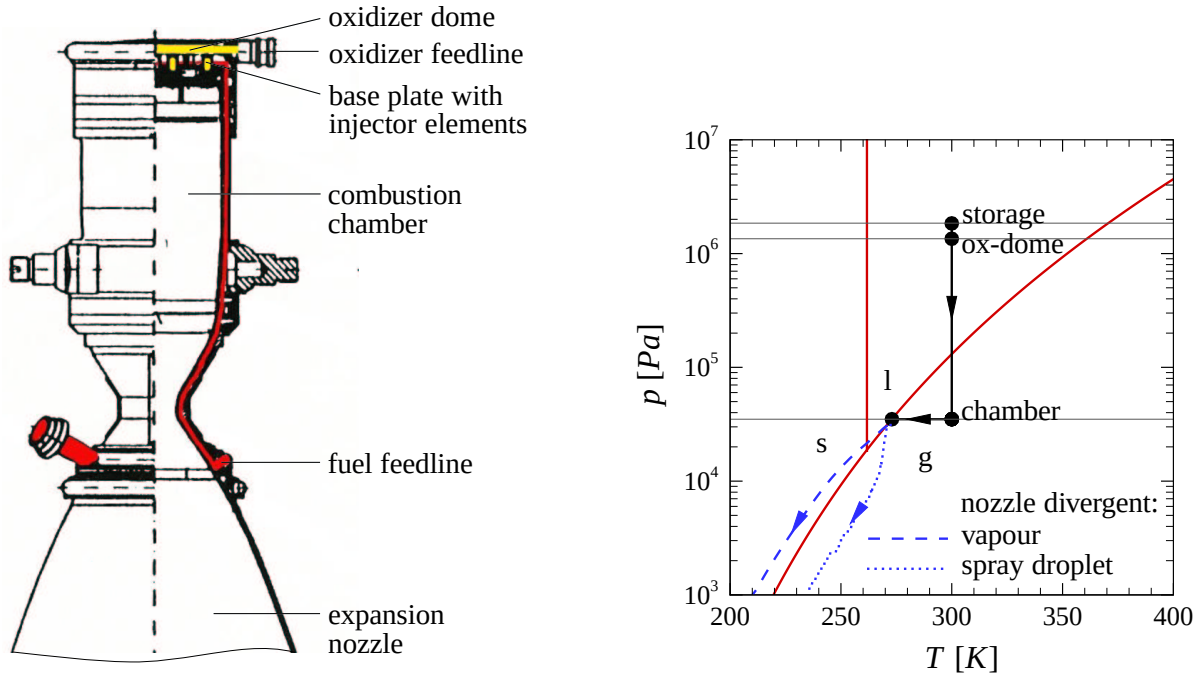

Figure 1: Core components of a hypergolic spacecraft engine (left), phase diagram of NTO (right)

bustion, this oxidizer preflow is characterized by thermodynamic conditions far from nominal operation of the engine. The pressure and temperature levels are predominantly controlled by the evaporation rate of the oxidizer. Due to the extreme pressure drop from oxidizer dome to combustion chamber (see figure 1, right) the injected liquid is superheated resulting in flash-atomization by rapid internal vapour formation and expansion. This mechanism is characterized by an extended spray cone and significantly reduced droplet sizes. Accordingly, heat and mass transfer between spray and vapour flow is governed by flash-evaporation. In contrast to conventional droplet evaporation, this mechanism is controlled by droplet internal transport of energy.

However, during preflow only a fraction of the injected oxidizer is evaporated in the subsonic chamber flow Aside of rapid spray transport and finite rate phase-change, this is mainly due to the limited superheat energy content and the absence of other energy sources. A considerable part of the spray deposits on the chamber walls. Evaporation and transport of this wall film depend on the thermal state of the wall, the shear stress on the vapour-film interface and body forces such as gravity or thrust. The remaining liquid phase fraction is accelerated in the divergent nozzle flow, where pressure and temperature experience a steep drop. In this region, the two-phase mixture is subject to significant non-equilibrium behaviour, as indicated in figure 1 by the phase-trajectories of metastable vapour (neglecting homogeneous condensation) and a flash-evaporating droplet.

The objective of the present study is a detailed 3D-CFD analysis of the oxidizer preflow in a generic spacecraft engine. Particular focus is on modelling issues associated with the low-pressure conditions, i.e. flash-atomization, flash-evaporation of spray and wall deposit as well as the intense phase interaction. Further, secondary breakup of droplets and spray-wall interaction are taken into account. Not considered are dissociation of the vapour phase, droplet-droplet interaction, transport and build-up of liquid wall film, homogeneous condensation and ice formation. The CFD-package METIS/Ladrop2 developed at the Institute for Thermal Turbomachinery, University of Karlsruhe, is used as a platform for model implementation and computational analysis.

2 Computational methodology

The general approach involves a finite volume method (METIS) to discretize the vapour flow and a Lagrangian droplet tracking method (Ladrop2) to describe spray dispersion. Since the vapour flow exclusively evolves from evaporation, two-way coupling between both phases is of major importance. As illustrated in figure 2, this coupling is realized by exchanging flow field data and spray source data data within an iterative procedure. To account for the transsonic character of the vapour flow, a compressible formulation of the SIMPLEC pressure correction scheme is used to describe the coupled pressure-velocity field [4]. The standard high-Reynolds number k-ε model is used by including additional transport equations for the turbulent kinetic energy k and its dissipation rate ε. Applying a contour-fitted finite volume discretization, the final equations can be cast into a general transport equation

$$a_P^{\phi}\phi_P = \sum_{nb} a_{nb}^{\phi}\phi_{nb} + S^{\phi,0} + S^{\phi,d}, \qquad \phi = p', u, v, w, h, k, \varepsilon, \quad (1)$$

where the volumes nb denote the neighbouring elements of each volume P. In this formulation, $S^{\phi,0}$ represents the constant part of the general source term and $S^{\phi,d}$ the spray source

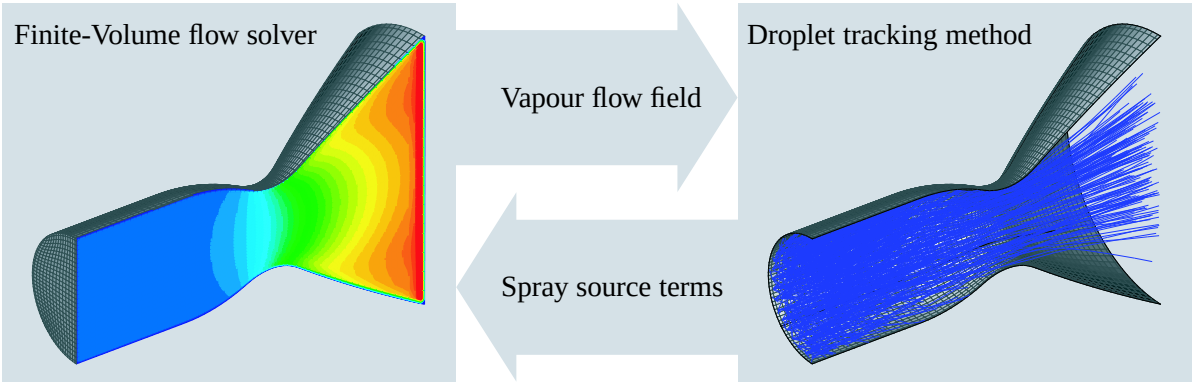

Figure 2: Iterative Euler-Lagrange method

term. The latter is derived by mapping of droplet trajectory data to the finite volume mesh

$$S^{m,d} = \sum_{k=1}^{N} f_k \left(m_d^{in} - m_d^{out} \right) , \quad S^{\phi,d} = \sum_{k=1}^{N} f_k \left(m_d^{in} \phi_d^{in} - m_d^{out} \phi_d^{out} \right) , \qquad \phi = u, v, w, h \, . \quad (2)$$

The quantities ϕ_d^{in} and ϕ_d^{out} represent droplet data on entry and exit of each discrete volume, f_k denotes the droplet number rate and N the total number of trajectories. Spray sources for the k-ε model are not considered in the present study. With respect to equation (1), the central coefficient is computed as

$$a_P^{p'} = \sum_{nb} a_{nb}^{p'} - S^{p',1} , \qquad a_P^{\phi} = \sum_{nb} a_{nb}^{\phi} - S^{\phi,1} + S^{m,d} , \qquad \phi = u, v, w, h, k, \varepsilon \, . \quad (3)$$

where the $S^{\phi,1}$ represent linear contributions to the general source term and $S^{m,d}$ a closing term linked to interphase mass transfer. It is important to note, that this correction is not applied to the central coefficient of the pressure-correction equation.
Due to the magnitude of the spray source terms, the following implementation scheme is crucial for stability of the iterative solver (BiCGSTAB):

- If $S^{\phi,d}$ and ϕ are of opposite sign, $S^{\phi,d}$ is not added to the right hand side of equation (1), but treated implicitly by substracting $S^{\phi,d}/\phi$ from a_P^{ϕ}.

- If $S^{m,d}$ is negative, $S^{m,d}$ is not added to a_P^{ϕ} as defined by equation (3), but treated explicitly by substracting $S^{m,d}\phi$ from the right hand side of equation (1).

In this way, spray source term contributions are consistently treated implicitly, when they enhance the diagonal dominance of the system matrix.
Due to its inherent suitability for detailed modelling of complex polydisperse sprays, a Lagrangian trajectory description is employed in the present study. The effect of turbulence on spray dispersion is simulated by stochastic generation of velocity fluctuations along the individual trajectories according to Gosman and Ioannides [2]. Wall impact of droplets is modelled by a detailed set of interaction mechanisms, including deposition, splashing, nucleate and film boiling as well as inelastic reflection. A detailed compilation of the theoretical framework is given in [7]. Modelling of droplet deformation and breakup by aerodynamic forces is taken into account by empirical correlations describing classification, temporal and spatial evolution as well as secondary fragment size spectra of various mechanisms [6].

3 Flash-atomization

During preflow, the coaxial injector elements operate as plain-orifice injectors in a flash-atomization mode. Compared to classical jet breakup, rapid internal vapour formation results in a burst-like expansion of the spray and significantly reduced droplet sizes. This effect is obvious from oxidizer spray visualizations of single injector elements indicating cone angles of about 100^o for preflow conditions - see figure 3. Although the influence of superheat and

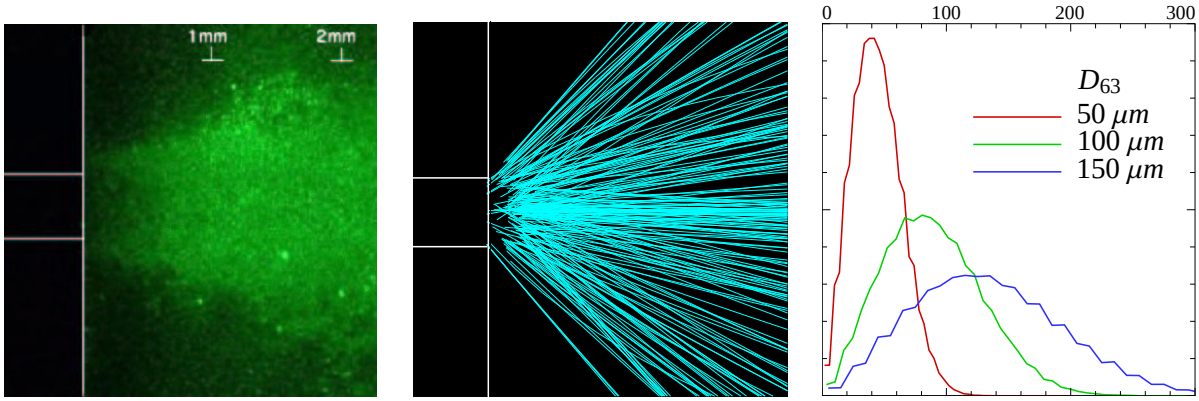

Oxidizer spray visualization [5] | Trajectory model, $\theta = N(\mu, \sigma)$ | Rosin-Rammler size distribution

Figure 3: Modelling plain-orifice flash-atomization by single injector elements

pressure drop within the injector has been quantified by various experimental studies, most of the data is not compiled in non-dimensional form. This is partly due to the complex dependency on phase change properties of the fluid and internal nozzle geometry. Consequently, experimental data based on test fluids should not be used for more than qualitative information on real propellant atomization: analyses of sprays with similar visual appearance, degrees of superheat and pressure drop indicate that maximum droplet diameters do not exceed 100 μm and Sauter mean diameters D_{32} range from 10 μm up to 50 μm [3, 5].
Figure 3 illustrates the stochastic description of oxidizer injection employed in the present study. The injection angle θ, measured from the injector axis, is generated from a clipped normal distribution with mean value, variance and maximum angle given in table 1. In this way,

n [−]	D_{63} [μm]	D_{32} [μm]
2.4	50	31.3
2.4	100	62.4
2.4	150	91.7

μ [^{o}]	σ [^{o}]	θ_{max} [^{o}]	$v_{d,0}$ [m/s]
0	45	50	19.8
$T_{d,0}$ [K]			
300			

Table 1: Parameters of the flash-atomization model used in the present study

droplet density is high on the axis and decreases towards the outer spray region. Droplet sizes are assumed to follow a Rosin-Rammler distribution. However, lacking specific information for preflow conditions, three different values for the diameter parameter D_{63} are investigated, leaving the width parameter n constant.
Based on this single injector model, a representative arrangement of injector elements on the base plate of the engine is reconstructed to simulate oxidizer injection in the engine configuration.

4 Droplet flash-evaporation

An essential component of the present study is an extension of classical D^2-theory to flash-evaporation of superheated droplets. The analytical framework is based on the assumption of spherical symmetric, quasisteady transport in the vapour phase. In this ideal case, the total heat flux $\dot{Q}$ and vapor mass flux $\dot{m}_{vap}$ leaving the droplet are both constant with respect to radial position. Thus, the quantities are interrelated by the differential energy balance in the vapour phase and the energy balance of the complete droplet (assuming uniform droplet temperature and denoting vapour phase properties without index)

$$\dot{Q} = \dot{m}_{vap}\, h(T) \;\; - \; 4\pi r^2 \lambda \frac{dT}{dr} \,, \qquad\qquad r > r_d \,, \tag{4}$$

$$\dot{Q} = \dot{m}_{vap}\, h_l(T_b) \; - \; m_d c_{p,l} \frac{dT_d}{dt} = -\frac{dH_d}{dt} \,. \tag{5}$$

Classical D^2-theory applies to a cold droplet in a hot vapour. Since the droplet is first heated up ($dT_d/dt > 0, \dot{m}_{vap} = 0$) and then evaporated at constant temperature ($dT_d/dt = 0, \dot{m}_{vap} > 0$), equation (4) can be solved by direct integration. For superheat conditions, the droplet surface spontaneously drops to the boiling temperature, evaporation is controlled by droplet internal heat transfer. For low superheat, $\Delta T = T_d - T_b$, conduction and convection are predominant. For higher ΔT, heat transfer is drastically increased by internal formation of vapour bubbles. Due to the complexity of these phenomena, a description based on an empirical heat transfer coefficient α_s is used to quantify internal heat flux $\dot{Q}_i$ and associated mass flux contribution $\dot{m}_{vap,f}$

$$\dot{Q}_i = 4\pi r_d^2 \, \alpha_s \, (T_d - T_b) = -m_d c_{p,l} \frac{dT_d}{dt} \,, \qquad\qquad \dot{m}_{vap,f} = \frac{\dot{Q}_i}{\Delta h_v} \,. \tag{6}$$

Making use of this definition, equation (4) can be integrated and results in an implicit expression for the total evaporation rate

$$\dot{m}_{vap} = 4\pi r_d \frac{\lambda^*_{ref}}{c_{p,ref}} \ln\left[1 + \frac{B_T}{1 - \frac{\dot{m}_{vap,f}}{\dot{m}_{vap}}}\right] , \qquad\qquad B_T = \frac{c_{p,ref}(T - T_b)}{\Delta h_v} \,. \tag{7}$$

Reference values λ_{ref} and $c_{p,ref}$ are evaluated at the temperature $T_{ref} = 2/3T_b + 1/3T$. The notation λ^*_{ref} includes an empirical correction taking into account forced convection in the vapour phase

$$\lambda^*_{ref} = cfh \; \lambda_{ref} \,, \qquad\qquad cfh = 1 + 0.276 \, \mathrm{Re}^{\frac{1}{2}} \, \mathrm{Pr}^{\frac{1}{3}} \,. \tag{8}$$

To quantify the heat transfer in the droplet, Zuo et al. [9] suggest a correlation derived from spray evaporation measurements in IC engines [1]

$$\alpha_s = \begin{cases} 760 \; \Delta T^{0.26} \,, & 0 \; K \le \Delta T \le \; 5 \; K \,, \\ 27 \; \Delta T^{2.33} \,, & 5 \; K < \Delta T \le 25 \; K \,, \\ 13800 \; \Delta T^{0.39} \,, & 25 \; K < \Delta T \,. \end{cases} \tag{9}$$

The present model further includes a size-dependent minimum value $\alpha_{s,min} = \lambda_l / r_d$ as an order of magnitude estimate for internal heat conduction.
Concluding, flash-evaporation of a droplet is described by the Lagrangian derivatives

$$\frac{dm_d}{dt} = -\dot{m}_{vap} \,, \qquad\qquad \frac{dT_d}{dt} = -\frac{\alpha_s \, 4\pi r_d^2}{m_d c_{p,l}} (T_d - T_b) \,. \tag{10}$$

Computations of flash-evaporating single droplets under typical preflow conditions have been reported in [8].

5 Spray-wall interaction

Deposition of spray depends on the local wall temperature. In the modelling framework, a threshold value of $T^* = 1.05\ T_b$ is used to separate the *cold wall* mechanisms droplet deposition and splashing (partial deposition) from the *hot wall* mechanisms nucleate boiling and, exceeding the Leidenfrost temperature, reflection [7]. Regarding superheated droplets, spontaneous phase change upon wall contact has to be taken into account. As a first approximation, the additional local effects are considered by assuming that initial wall deposit flash-evaporates to a degree where the remaining deposit is at the local boiling temperature.
During start-up of the engine, wall temperatures experience an extreme transition first adapting to the cold oxidizer preflow and then to the hot reacting flow. Since experimental temperature data is not available, a sensitivity analysis has been performed to study the effect of boundary conditions, including isothermal and adiabatic walls. It shows that the global character of the flow does not change significantly for wall temperatures below T^*. Exceeding this value, transition to nucleate boiling of wall deposit occurs. Since modelling of this complex mechanism is idealized as complete evaporation by heat transfer from the wall, vapour release increases drastically in this regime tending to block the nozzle which in turn increases pressure and temperature in the combustion chamber.
Concluding the analysis, adiabatic conditions are choosen for the present flow computations, assuming that wall temperatures during preflow are below T^* and thus determined by cold wall interaction mechanisms. The decision is supported by computed pressure levels.

6 Results

Using the oxidizer NTO (Nitrogen Tetroxide) typically employed in spacecraft propulsion, the computed preflow is presented for the three initial size spectra summarized in table 1. The computational domain illustrated in figure 2 (left) is discretized by $68 * 29 * 15$ finite volumes, the primary sprays from flash-atomization by 70000 trajectories per vapour-spray iteration. Depending on the initial size spectrum, trajectories of secondary droplets double to triple this number. To ensure stability of the iterative Euler-Lagrange method, underrelaxation of spray source terms by $\overline{S}_i = \alpha S_i + (1-\alpha) S_{i-1}$ is required, applying $\alpha = 5\%$.

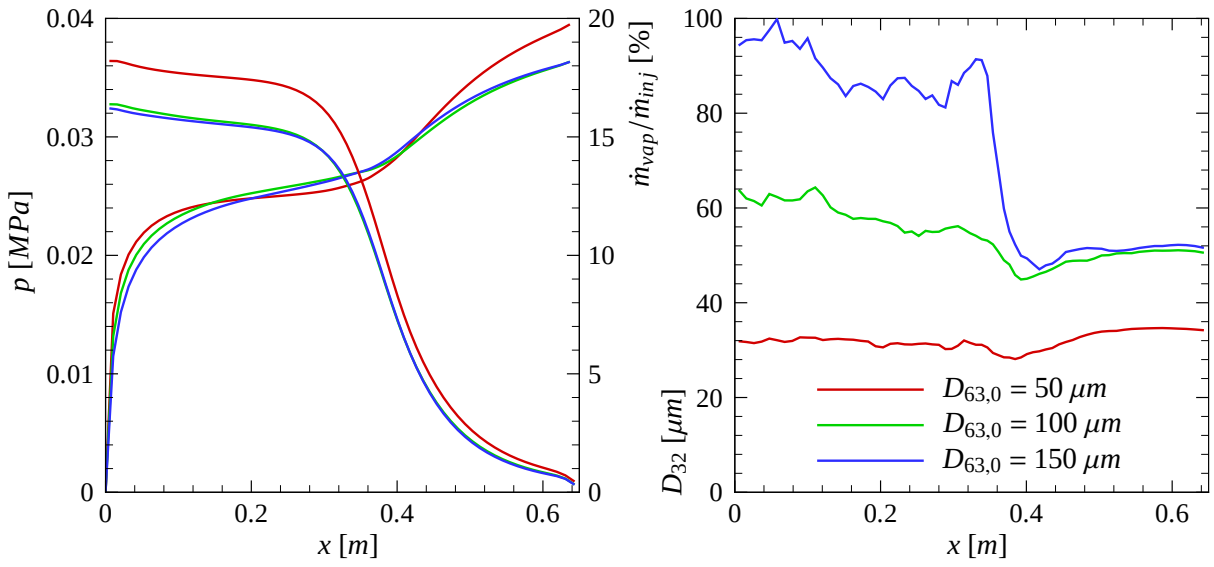

Figure 4: Pressure on axis and evaporated mass fraction (left), Sauter mean diameter on axis (right)

As illustrated in figure 4, static pressure in the combustion chamber is nearly constant and slightly decreases towards the throat due to increasing flow velocity. Correspondingly, the vapour mass flow approaches a nearly constant value in the chamber due to rapid phase transfer by flash-atomization and evaporation within a short distance from the base plate. Further evaporation is associated to the steep pressure drop in the nozzle divergent. The evolution of mass flow indicates an effect of droplet size. The decreasing inertia of small droplets with respect to phase transfer has a pronounced effect for the 50 μm-spray, causing a step-like increase in mass flow to a plateau and a further steep increase in the nozzle divergent.

The total effect of spray physics on the size spectrum is characterized by the evolution of the Sauter mean diameter D_{32}. Up to the throat, D_{32} slightly decreases in the mean. Fluctuations are more pronounced for the coarse spray, which, due to the wide angle character and the distinct inertia of large droplets is more prone to wall-impingement. On the other hand, the fine spray rapidly adapts to the chamber flow. Accordingly, wall-interaction and to a lesser extent aerodynamic droplet breakup are responsible for the substantial drop of D_{32} in the throat region. Effectively, the nozzle acts on droplet size as a low-pass filter. In this context it is interesting to note, that the pressure level in the chamber appears to be correlated with the vapour mass flow in throat and nozzle divergent, which, due to the filtering effect, is very similar for the 100 μm and 150 μm-sprays.

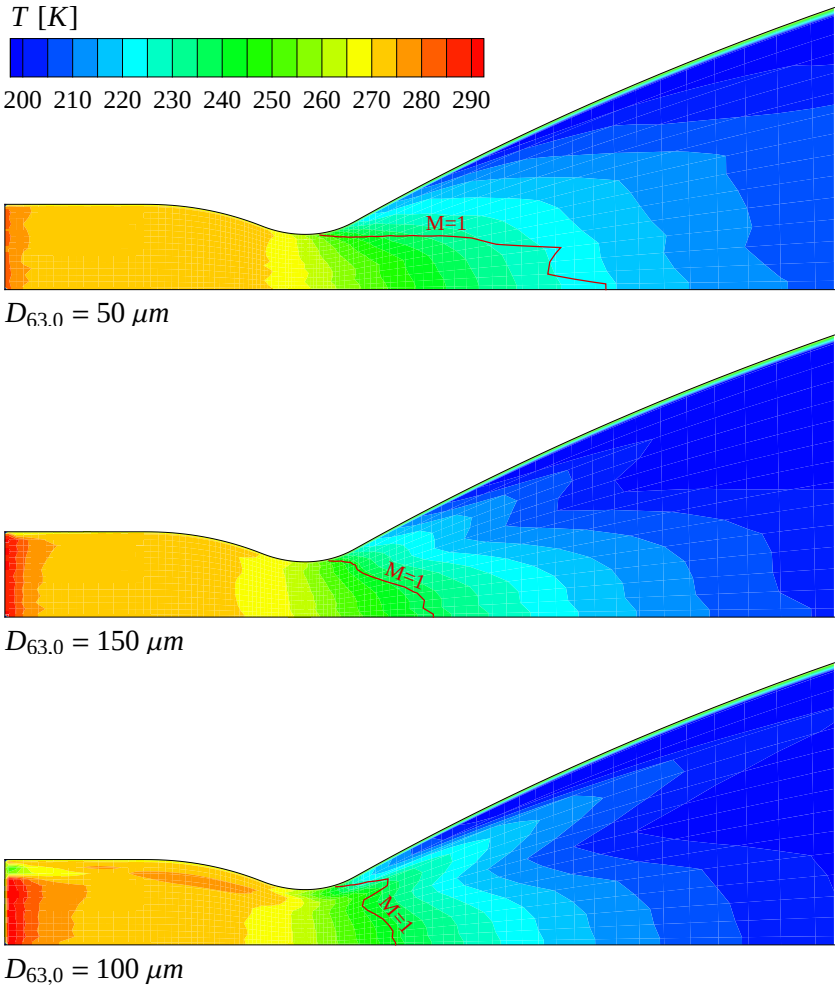

Figure 5: Vapour temperature and sonic line in longitudinal section of chamber and nozzle

Contour plots of static temperature are depicted in figure 5. For the fine spray a nearly homogeneous distribution in the chamber is achieved. The coarse spray is characterized by significant temperature streaks indicating the downstream evaporation effect of individual spray plumes. Spots of elevated static temperatures occur towards the base plate which can be attributed to low flow velocities due to delayed vapour formation (see also figure 4, left). As indicated by the sonic lines, the subsonic region of the two-phase flow tends to expand into the divergent part of the nozzle. This effect is most pronounced for the fine spray.
Spray deposition on chamber walls is characterized by a bimodal character. As illustrated in figure 6, liquid oxidizer is deposited on the cylindrical part of the liner mainly due to spray impingement from the peripheral row of injector elements. Caused by wide-angle flash-atomization of the injected liquid, this massive spray deposition significantly contrasts the behaviour at nominal operation of the engine. A second region of increased deposition occurs at the converging part of the nozzle. This effect is mainly due to larger spray components which are not able to follow the contracting flow (compare D_{32} in figure 4). The global distribution

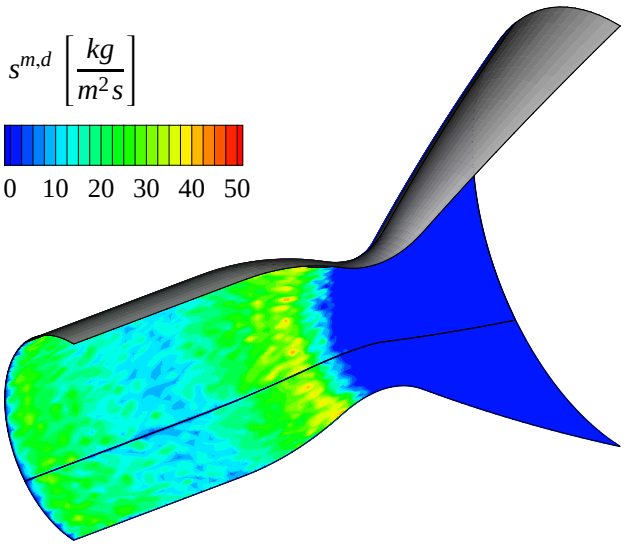

Averaged deposited mass flux $\dot{m}$ $[kg/s/m^2]$:

$D_{63,0}$ $[\mu m]$	50	100	150
Baseplate	0	0	0
Cylindrical part	13.38	18.00	18.65
Converging part	18.09	22.79	20.98

Figure 6: Deposition mass flow density for the 150 μm-spray (left) and mass flow distribution (right)

of liquid mass deposit is given in the side-table of figure 6, illustrating the dependency on the initial size spectrum. Accumulation on the base plate could not be assessed in the present study due to the limited resolution of the computational grid which does not allow for capturing of small-scale recirculation zones and hence the possible entrapment and deposition of droplets.

7 Conclusions

The low-pressure oxidizer preflow in a hypergolic spacecraft engine is characterized by intense phase transfer due to flashing of injected superheated liquid. The presented computational analysis addresses this issue by an empirical description of flash-atomization and a semi-empirical extension of D^2-theory to flash-evaporation of individual spray droplets. A consistent implementation of spray source terms ensures numerical stability of the flow solver within the coupled Euler-Lagrange approach. The analysis indicates that pressure and temperature level in the chamber are further controlled by spray-wall interaction including flash-evaporation of wall-deposit. It is demonstrated that the typical wide-angle character from

flash-atomization causes massive oxidizer deposition on the cylindrical part of the combustion chamber. Further improvement of the analysis can be expected from detailed research on flashing phenomena and development of physical models.

Acknowledgements

The authors acknowledge the interest and support of ESA for this research activity which is conducted at ESTEC in the frame of an internal research fellowship.

References

[1] M. Adachi, V. G. McDonell, D. Tanaka, J. Senda, and H. Fujimoto. Characterization of fuel vapor concentration inside a flash boiling spray. *SAE Paper 970871*, 1997.

[2] A. D. Gosman and E. Ioannides. Aspects of Computer Simulation of Liquid-Fueled Combustors. *Journal of Energy*, 7(6):482–490, 1983.

[3] E. Hervieux and T. Veneau. Experimental determination of the droplet size and velocity distributions at the exit of the bottom discharge pipe of a liquefied propane storage tank during a sudden blowdown. *J. Loss Prev. Process Ind.*, 9(6):413–425, 1998.

[4] K. Karki and S. Patankar. Pressure based calculation procedure for viscous flows at all speeds in arbitrary configurations. *AIAA-Journal*, 27:1167–1174, 1989.

[5] L. Pouvreau, T. Yoshizaki, and K. Nishida. Atomization of a Heated Liquid Jet: Enhancement of Breakup and Dispersion through a Hole Nozzle. In *8th International Conference on Liquid Atomization and Spray Systems, ICLASS 2000, Pasadena, USA*, 2000.

[6] R. Schmehl, G. Maier, and S. Wittig. CFD Analysis of Fuel Atomization, Secondary Droplet Breakup and Spray Dispersion in the Premix Duct of a LPP Combustor. In *8th International Conference on Liquid Atomization and Spray Systems, ICLASS 2000, Pasadena, USA*, 2000.

[7] R. Schmehl, H. Rosskamp, M. Willmann, and S. Wittig. CFD Analysis of Spray Propagation and Evaporation Including Wall Film Formation and Spray/Film Interactions. *International Journal of Heat and Fluid Flow*, 20:520–529, 1999.

[8] R. Schmehl and J. Steelant. Evaluation of Oxidizer Temperature Drop in a Combustion Chamber. In *4th International Conference on Launcher Technology "Space Launcher Liquid Propulsion", Liège, Belgium*, 2002.

[9] B. Zuo, A. Gomes, and C. J. Rutland. Studies of superheated fuel spray structures and vaporization in GDI engines. 11th International Multidimensional Engine Modeling User's Group Meeting, http://www.erc.wisc.edu, 2001.